GABAergic inhibition at dendrodendritic synapses tunes γ oscillations in the olfactory bulb

Samuel Lagier[†], Patrizia Panzanelli[‡], Raúl E. Russo[†§], Antoine Nissant[†], Brice Bathellier[†¶], Marco Sassoè-Pognetto[‡‖], Jean-Marc Fritschy[††], and Pierre-Marie Lledo[†‡‡]

[†]Laboratory of Perception and Memory, Centre National de la Recherche Scientifique, Unité de Recherche Associée 2182, Institut Pasteur, 25 Rue du Dr. Roux, F-75724 Paris Cedex 15, France; [‡]Department of Anatomy, Pharmacology, and Forensic Medicine and [‖]Istituto Nazionale di Neuroscienze, University of Turin, I-10126 Turin, Italy; [¶]Laboratory of Computational Neuroscience, Brain and Mind Institute, Ecole Polytechnique Fédérale de Lausanne, CH-1015 Lausanne, Switzerland; [††]Institute of Pharmacology and Toxicology, University of Zurich, CH-8057 Zurich, Switzerland; and [§]Neurofisiolgía Celulary Molecular, Instituto de Investigaciones Biológicas, Clemente Estable, Avenida Italia 3318, CP 11600 Montevideo, Uruguay

Communicated by D. Carleton Gajdusek, Institut de Neurobiologie Alfred Fessard, Gif-sur-Yvette, France, March 5, 2007 (received for review November 7, 2006)

In the olfactory bulb (OB), odorants induce oscillations in the γ range (20–80 Hz) that play an important role in the processing of sensory information. Synaptic transmission between dendrites is a major contributor to this processing. Glutamate released from mitral cell dendrites excites the dendrites of granule cells, which in turn mediate GABAergic inhibition back onto mitral cells. Although this reciprocal synapse is thought to be a key element supporting oscillatory activity, the mechanisms by which dendrodendritic inhibition induces and maintains γ oscillations remain unknown. Here, we assessed the role of the dendrodendritic inhibition, using mice lacking the $GABA_A$ receptor α1-subunit, which is specifically expressed in mitral cells but not in granule cells. The spontaneous inhibitory postsynaptic current frequency in these mutants was low and was consistent with the reduction of $GABA_A$ receptor clusters detected by immunohistochemistry. The remaining $GABA_A$ receptors in mitral cells contained the α3-subunit and supported slower decaying currents of unchanged amplitude. Overall, inhibitory-mediated interactions between mitral cells were smaller and slower in mutant than in WT mice, although the strength of sensory afferent inputs remained unchanged. Consequently, both experimental and theoretical approaches revealed slower γ oscillations in the OB network of mutant mice. We conclude, therefore, that fast oscillations in the OB circuit are strongly constrained by the precise location, subunit composition and kinetics of $GABA_A$ receptors expressed in mitral cells.

α1 knockout | $GABA_A$ receptor | olfaction | reciprocal synapses

In the olfactory bulb (OB), γ frequency (20–80 Hz) oscillations of local field potentials (LFP) reflect synchronized spike discharges of principal neurons (i.e., mitral/tufted cells), and may be part of the encoding of sensory information (reviewed in refs. 1 and 2). In line with this assumption, the strength of γ oscillations correlates with both discrimination abilities (3) and learning capacities (4, 5) in rodents.

In vivo experimental approaches revealed that γ oscillations are intrinsic to the OB circuitry (5–7) and are even preserved in slice preparations (8, 9), which suggests that intrinsic properties of the OB connectivity are sufficient to give rise to large-scale synchronization. Analysis of the mechanisms involved has focused almost exclusively on the excitatory principal neurons (i.e., mitral cells) and included intrinsic subthreshold oscillations (10, 11) or mutual excitation through electrical coupling and glutamate spillover between mitral cells sharing the same glomerulus (12–14). As a result, relatively little is known about the role of local inhibitory interneurons in generating and maintaining network oscillations, although pioneering studies proposed dendrodendritic inhibition as a key element for inducing fast rhythms (15–17). This assumption is also supported by the fact that interneurons constitute the main target of excitatory centrifugal fibers (18, 19) known to control oscillatory activities in the OB circuitry (5).

Here, we exploited the differential expression pattern of $GABA_A$ receptor subunits in OB neurons to selectively manipulate dendrodendritic inhibition. $GABA_A$ receptors are composed of five subunits, most frequently two α-, two β-, and one γ-subunit. The combination of different subunits gives rise to a large diversity of $GABA_A$ receptors (reviewed in ref. 20) that are differentially expressed in the brain and localized in different cell types and/or subcellular areas (21). In the OB network, mitral cells selectively express $GABA_A$, receptors containing the α1- and/or the α3-subunits, whereas GABAergic granule cells express the α2- and α5-subunits (22). Thus, we predicted that after genetic deletion of the α1-subunit ($\alpha 1^{0/0}$) (23), functional $GABA_A$ receptors would be altered in a cell type-specific manner. This targeted manipulation of inhibition allowed us to investigate the precise involvement of dendrodendritic inhibition for the generation and maintenance of fast oscillations in the OB circuitry.

Results

Specific Reorganization of $GABA_A$ Receptors in $\alpha 1^{0/0}$ Mitral Cells. Double and triple immunofluorescence staining for gephyrin, a marker of inhibitory postsynaptic sites, and the $GABA_A$ receptor α1-, α2-, α3-, and α5-subunits were performed in WT and $\alpha 1^{0/0}$ mice to investigate how the loss of the α1-subunit might affect the distribution of GABAergic synapses [Fig. 1 and supporting information (SI) Figs. 7 and 8]. In sections from both $\alpha 1^{0/0}$ and WT mice, numerous brightly stained gephyrin clusters were distributed across the external plexiform layer (EPL) and no difference in distribution was detectable between genotypes (Fig. 1*A1* and *B2*). In both cases, their density varied between 190 and 250 per 1,000 μm^2 (SI Table 1). Likewise, the dimension of gephyrin clusters as quantified by cumulative distribution analysis was also the same in both genotypes (SI Figs. 7*A1* and 8*A1*). In contrast to gephyrin, a genotype effect on the distribution of α3-subunit-positive clusters was evident. In WT mice, staining was most prominent in the outer EPL (Fig. 1*A2*), whereas the α3-subunit was redistributed in mutant mice to become uniform across the EPL (Fig. 1*B1*), similar to the WT distribution of the α1-subunit (Fig. 1*C*). These findings suggest that GABAergic

Author contributions: S.L., P.P., J.-M.F., and P.-M.L. contributed equally to this work; M.S.-P., J.-M.F., and P.-M.L. designed research; S.L., P.P., R.E.R., A.N., B.B., and J.-M.F. performed research; S.L., A.N., B.B., M.S.-P., and P.-M.L. analyzed data; and S.L., J.-M.F., and P.-M.L. wrote the paper.

The authors declare no conflict of interest.

Abbreviations: DDI, dendrodendritic inhibition; EPL, external plexiform layer; GCL, granule cell layer; IPSC, inhibitory postsynaptic current; LFP, local field potentials; OB, olfactory bulb; sIPSC, spontaneous inhibitory postsynaptic current; uIPSC, unitary inhibitory postsynaptic current.

[‡‡]To whom correspondence should be addressed. E-mail: pmlledo@pasteur.fr.

This article contains supporting information online at www.pnas.org/cgi/content/full/0701846104/DC1.

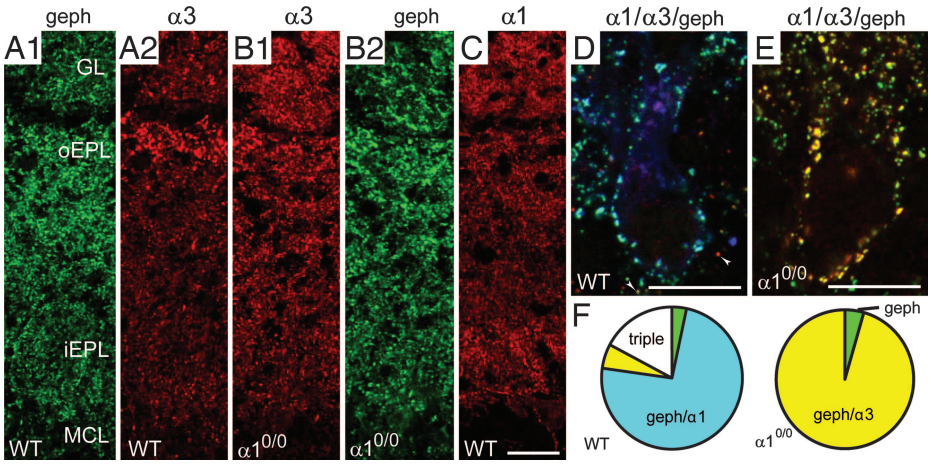

Fig. 1. Reorganization of $GABA_A$ receptor subtypes in $\alpha1^{0/0}$ mice. (*A–C*) Double staining for gephyrin (*A1* and *B2*) and the α3-subunit (*A2* and *B1*) in WT and mutant ($\alpha1^{0/0}$) mice reveals no change in gephyrin distribution and a stronger and more uniform α3-subunit immunoreactivity in the mutant, resembling the distribution of the α1-subunit in WT (*C*). (Scale bar: 50 μm.) (*D* and *E*) Triple staining of mitral cells for gephyrin (green), α1- (blue), and α3-subunit (red). In WT, α1-subunit-positive clusters colocalize with gephyrin on the soma and a few α3-subunit-positive clusters are present in the vicinity (arrowheads). In $\alpha1^{0/0}$ mice, extensive colocalization of the α3-subunit with gephyrin results in a yellow staining in the overlay. (*F*) Quantification of the types of clusters found on the soma of mitral cells in WT and mutant mice. Colors correspond to the staining patterns shown in *D* and *E*. (Scale bars: 10 μm.)

synapses are preserved in $\alpha1^{0/0}$ mice and more often contain α3-$GABA_A$ receptors than in WT.

Higher magnification showed the majority of α3 subunit-positive clusters to be colocalized with gephyrin, in both WT and mutant mice (SI Fig. 8 *A* and *B*). Gephyrin clusters devoid of α3-subunit labeling were also detected, probably associated with other $GABA_A$ receptor subtypes. This possibility was tested by a systematic quantitative analysis of sections labeled for gephyrin and either α1, α2, α3, or α1/α3 (see SI Table 1). In WT mice, the total number of α subunit clusters associated with gephyrin was about the same as the total number of gephyrin clusters. The second most abundant subunit in WT is α3; this subunit might be overexpressed to compensate for the loss of α1. However, the number of α3 subunit-positive clusters in $\alpha1^{0/0}$ mice was slightly, although not significantly, higher (+31% and + 24% in the inner and outer EPL, respectively). Nevertheless, α3-subunit clusters were more intensely stained and found to be larger than in WT (SI Fig. 7 *B1* and *B2*), accounting for the difference in distribution seen at low magnification. No change in the distribution and abundance of α2- and α5-subunit-immunofluorescence was detected in mutant mice (SI Fig. 8 *E–J*). These findings suggested that "orphan" gephyrin clusters corresponded to incomplete, nonfunctional postsynaptic sites.

A different result was obtained in the mitral cell body layer where mitral cell somatas receive a strong GABAergic innervation from granule cell dendrites to control neuronal excitability and output patterns. As in the EPL, there were no differences in the number of gephyrin clusters between the two genotypes (14.5 ± 5 clusters per mitral cell profile in WT versus 13.8 ± 6 in $\alpha1^{0/0}$ mice; mean ± SD, $n = 59$ and 54 cells, respectively; not significant, *U* test). In WT mice, most of these clusters (74%) contained only the α1-subunit, 6% contained only the α3-subunit, and 17% contained both subunits. In contrast, in $\alpha1^{0/0}$ mice, nearly all gephyrin clusters contained the α3-subunit (Fig. 1 *D–F*). Thus, an increase in abundance of the α3-subunit fully compensates for the absence of α1-subunit in GABAergic synapses formed on mitral cell somata. An important consequence is the presence of gephyrin clusters free of α subunits solely on mitral cell dendrites, which might be nonfunctional postsynaptic sites. These results suggest that the interchangeability of α1- and α3-subunits strongly depends on the location (somatic versus dendritic), and possibly the function, of the inhibitory synapses involved.

Preservation of Reciprocal Synapses in the EPL of $\alpha1^{0/0}$ Mice. We next used electron microscopy to investigate possible changes in the morphology of reciprocal dendrodendritic synapses in the EPL. Immunogold labeling for GABA showed no difference between mutant and WT mice (Fig. 2 *A1* and *A2*). Likewise, labeling for gephyrin, which was concentrated at postsynaptic specializations of symmetric synapses (24), showed a similar distribution of gold particles in both genotypes (Fig. 2 *B1* and *B2*). Finally, immunogold staining for α3-subunits revealed a much stronger immunoreactivity in $\alpha1^{0/0}$ versus WT mice at symmetric synaptic specializations (Fig. 2 *C1–C3*; see SI Fig. 7*C* for quantification). Interestingly, labeling for the α3-subunit was also seen presynaptically at asymmetric junctions in both genotypes, as reported for the α1-subunit (25). These results clearly show that the absence of the α1-subunit does not result in a morphological impairment of GABAergic synapses or a redistribution of gephyrin to other sites. We next used electrophysiological methods applied on acute OB slices to assess the functional consequences of these anatomical alterations.

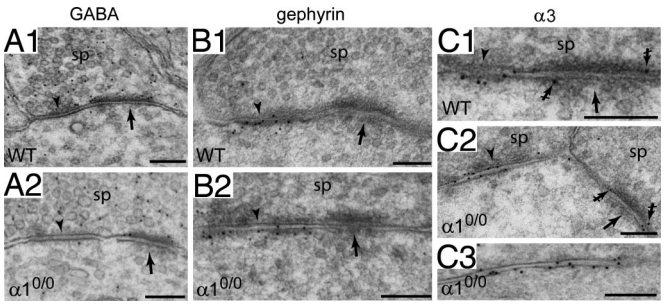

Fig. 2. Ultrastructural characterization of dendrodendritic synapses in the EPL of $\alpha1^{0/0}$ mice (postembedding immunogold labeling). (*A1* and *A2*) GABA labeling in WT and mutant ($\alpha1^{0/0}$) mice, depicting the normal morphology of dendrodendritic synapses between granule cell spines (sp) and mitral cell dendrites. Arrowheads point to the symmetric (GABAergic) synapses and arrows to the asymmetric (glutamatergic) synapses. (*B1* and *B2*) Gephyrin labeling, showing the selective aggregation of gold particles on the postsynaptic site of the symmetric synapse (arrowheads) and the absence of labeling of the asymmetric synapse (arrows) in both genotypes. (*C1–C3*) α3-subunit labeling in both the symmetric (arrowheads) and asymmetric (crossed arrows) synapses in either genotype. (Scale bars: 200 nm.)

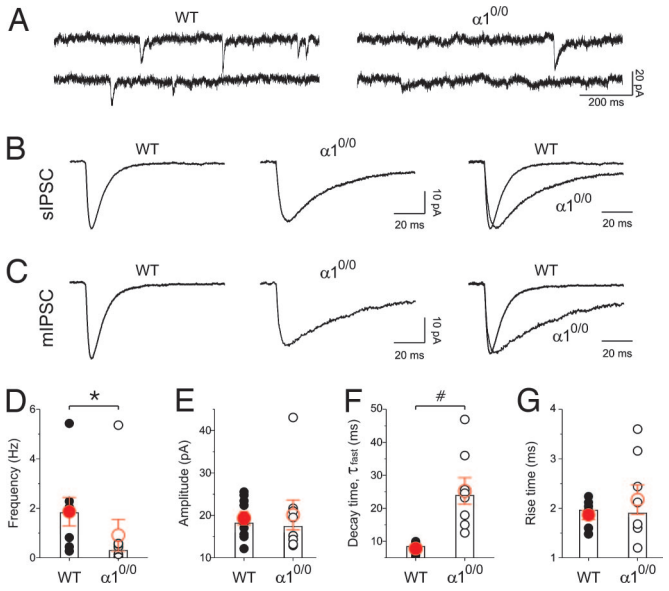

Fig. 3. Synaptic GABAergic events in mitral cells are less frequent and decay slower in $\alpha1^{0/0}$ than in WT mice. (*A*) Recordings of sIPSCs in a mitral cell from a WT (WT) (*Left*) or a mutant ($\alpha1^{0/0}$) (*Right*) mouse, in the presence of 5 mM kynurenate and 20 μM gabazine. (*B*) Mean sIPSCs obtained from the cells presented in *A*. The traces are scaled in at *Right*. (*C*) Mean miniature IPSCs (mIPSCs) recorded as in *A* with 1 μM tetrodotoxin. (*D*) Distribution of sIPSC frequency in WT (solid circles) and $\alpha1^{0/0}$ (open circles) mice. Columns represent the median of the distributions, red circles and error bars represent the mean and SEM, respectively. (*E*) Distribution of sIPSC amplitude. (*F*) Distribution of the fast component of sIPSC decay. See also SI Fig. 8 for further analyzes. (*G*) Distribution of sIPSC rise time (10–90% of the total amplitude). *, $P < 0.05$; #, $P < 0.001$, Mann–Whitney test, $n = 9$ and 8 cells for WT and $\alpha1^{0/0}$, respectively.

Less Frequent Inhibitory Synaptic Events with Slower Decay in $\alpha1^{0/0}$ Mitral Cells. First, we recorded spontaneous inhibitory postsynaptic currents (sIPSCs) from mitral cells under the whole-cell voltage-clamp configuration. The mitral cells were held at −70 mV and symmetrical Cl^- concentrations were used (*SI Methods*) so that $GABA_A$ receptor-mediated currents were inward (Fig. 3 *A* and *C*). In the WT, sIPSCs occurred with a mean frequency of 1.86 ± 0.58 Hz and amplitude of 19.3 ± 0.6 pA ($n = 8$). In $\alpha1^{0/0}$ mice, sIPSC frequency was 50% lower (Fig. 3 *A* and *D*; 0.91 ± 0.64 Hz; $n = 8$; $P < 0.05$, *U* test) but the amplitude remained unchanged (20.1 ± 3.5 pA; not significant; Fig. 3 *B* and *E*). The reduction in sIPSC frequency was accompanied by an increase in their decay time (Fig. 3*B*): fast time constant was 7.8 ± 0.6 ms in WT and 25.2 ± 4.0 ms in $\alpha1^{0/0}$ mice (Fig. 3*F*; $P < 0.001$, *U* test). The relative contribution of the fast to the slow component of the sIPSCs decay time was lower in the mutant mice (SI Fig. 9). In contrast, the 10–90% rise time did not differ between the two animal groups (1.87 ± 0.09 ms and 2.17 ± 0.30 ms for WT and $\alpha1^{0/0}$ mice, respectively; Fig. 3*G*) indicating that the passive conductance properties of the mitral cells and the location of functional GABAergic synapses in $\alpha1^{0/0}$ mice were similar. In contrast, sIPSCs recorded from granule cells were not significantly different in WT and $\alpha1^{0/0}$ mice ($n = 10$; SI Fig. 10), thus indicating that the observed changes of inhibitory currents were restricted to mitral cells. From these anatomical and physiological evidence, we concluded that the specific loss of the $\alpha1$-subunit from mitral cells led to a dramatic reduction of functional GABAergic synapses on mitral cell dendrites and to slower decaying sIPSCs. Because of the rarity of inhibitory synaptic events recorded in the presence of tetrodotoxin in $\alpha1^{0/0}$ mice (<1 event per minute), we could not perform a quantitative investigation of miniature IPSCs. Nevertheless, average miniature IPSCs from mitral cells are shown in Fig. 3*C* to compare their kinetics.

Slower Dendrodendritic Inhibition in $\alpha1^{0/0}$ Mitral Cells. To characterize further the inhibitory synaptic transmission in $\alpha1^{0/0}$ mice, we measured evoked GABAergic responses mediated by dendrodendritic reciprocal synapses between granule and mitral cells. To evoke dendrodendritic inhibition (DDI), we applied a brief (50 ms) depolarizing step from −70 to + 10 mV that elicited a typical barrage of synaptic events in mitral cells (Fig. 4*A*) (*SI Methods*). Recordings were first initiated in standard conditions and then in

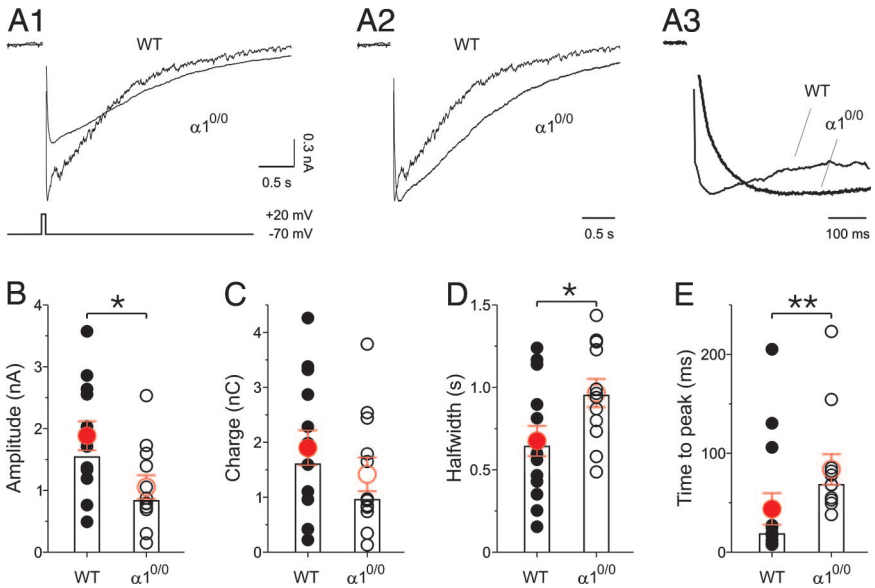

Fig. 4. DDI is smaller and slower in the absence of $\alpha1$-subunit. (*A1*) Average DDI in mitral cells from a WT and a mutant ($\alpha1^{0/0}$) mouse. The voltage step is represented below the sweeps. DDI responses are calculated by subtracting the average response recorded in the presence of gabazine from the average response recorded in ACSF. (*A2*) Superimposition of the scaled sweeps from *A1*. (*A3*) Same traces as in *A2* at a faster time scale to show the onset of the DDI response. (*B*) Distribution of DDI amplitude in WT (solid circles) and $\alpha1^{0/0}$ (open circles) mice. Columns represent the median of the distributions, and red circles and error bars represent the mean and SEM, respectively. (*C*) Distribution of DDI charge. (*D*) Distribution of DDI half-width. (*E*) Distribution of DDI time to peak. *, $P < 0.05$; **, $P < 0.01$, Mann–Whitney test, $n = 14$ and 12 cells for WT and $\alpha1^{0/0}$, respectively.

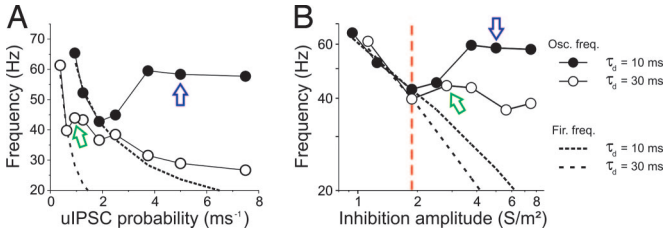

Fig. 5. Simulation of the $\alpha1^{0/0}$ phenotype in a network model. (*A*) Changes in the network oscillation frequency according to changes in release probability peak amplitude for a "WT"-like model (solid circles; decay time of uIPSC of 10 ms) and a "$\alpha1^{0/0}$"-like model (open circles; decay time of 30 ms). The dashed lines represent mitral cells firing frequency under the same conditions. The arrows (blue for WT and green for $\alpha1^{0/0}$) point to the values used in SI Fig. 11*F*. (*B*) Changes in the network oscillation frequency according to changes in inhibition for the same two networks as in *A*. Recurrent and lateral inhibition are changed proportionally. The red dashed line figure the threshold in inhibition amplitude below which the oscillation frequency equal the mitral cells firing frequency for both networks. The legends are the same for the two graphs.

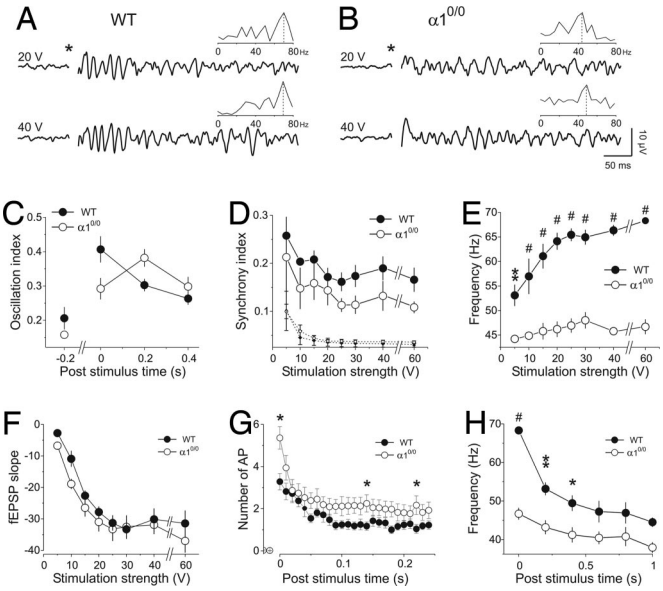

Fig. 6. Network properties in WT and $\alpha1^{0/0}$ mice. (*A*) LFP recordings in a slice from a WT (WT) mouse at 20 V (*Upper*) and 40 V (*Lower*). The star indicates the onset of olfactory nerve stimulation. (*B*) LFP recordings from $\alpha1^{0/0}$ OB slice at 20 V (*Upper*) and 40 V (*Lower*). (*C*) Changes in the oscillation index over time, for a 60 V stimulation, from WT (solid circles) and $\alpha1^{0/0}$ (open circles) mice. (*D*) Plot of the synchrony index against the stimulation strength. This index was always higher in WT mice, but this apparent difference is not significant. The small open and solid circles and dashed lines at the bottom of the plot represent the theoretical values of the index for a uniform spike phase distribution given the number of recorded spikes. (*E*) Frequency of LFP oscillations at various stimulation strengths, computed during the 200 ms after stimulation. (*F*) Evolution of the slope of field excitatory postsynaptic potential recorded next to the mitral cell layer in acute OB slices. (*G*) Poststimulus time histogram of mitral cell activity evoked with a 60 V olfactory nerve stimulation. (*H*) Evolution of LFP oscillation frequency over time evoked with a 60 V stimulation. *, $P < 0.05$; **, $P < 0.01$; #, $P < 0.005$; ANOVA with repeated measures; $n = 6$ for both WT and $\alpha1^{0/0}$ mice.

the presence of gabazine (20 μM) to isolate the GABAergic compound by subtraction. To quantify the DDI, we measured both the amplitude and the integral of the subtracted current. In $\alpha1^{0/0}$ mice, this response was smaller (Fig. 4*A1* and *B*; 1.88 ± 0.23 nA and 1.05 ± 0.19 nA for WT and $\alpha1^{0/0}$, respectively; $P < 0.05$ with a Mann–Whitney test, $n = 14$ and 12 cells for WT and $\alpha1^{0/0}$, respectively). The decrease in amplitude was accompanied with broader responses characterized by longer half-width (Fig. 4*A2* and *D*; from 675 ± 91 ms to 966 ± 85 ms; $P < 0.05$ with a Mann–Whitney test) and longer rise time (Fig. 4*E*; time to peak: 43 ± 16 ms and 84 ± 15 ms for WT and $\alpha1^{0/0}$ mice, respectively; $P < 0.01$ with a Mann–Whitney test). As a result, the reduced amplitude combined with a longer duration led to unchanged current charges in mutant animals (Fig. 4*C*; 1.90 ± 0.32 nC and 1.42 ± 0.31 nC for WT and $\alpha1^{0/0}$, respectively). Thus, evoked inhibition between mitral cells and inhibitory interneurons was slower to rise and to decay, and had smaller amplitude in $\alpha1^{0/0}$ mice. Yet, the total charges transfer of reciprocal GABAergic responses remained unchanged.

Fewer GABAergic Events Degrade Fast Oscillations in a Network Model. To infer the role of GABAergic synaptic inhibition in controlling synchronous network activity, we designed a physiologically based network model of the OB circuit that contains 100 heterogeneous MCs (26) and receiving olfactory nerve inputs. This network model includes the main synaptic interactions (lateral excitation and inhibition) and recurrent action (autoexcitation and recurrent inhibition) and takes into account two major features of the OB of $\alpha1^{0/0}$ mice: the reduced number of functional dendrodendritic synapses and the prolongation of their recurrent inhibitory component (SI Fig. 11). The first feature was mimicked by a reduction in the inhibitory event occurrence probability (i.e., the average number of unitary events in a reciprocal or lateral IPSC, which obviously depends on the number of functional synapses involved in the inhibitory response; see ref. 26), and the second characteristic by a three-fold increase in the decay time of unitary IPSC (uIPSC) (see Fig. 3*F*). The reduction of the inhibitory event occurrence probability (uIPSC probability) was calculated to halve the amplitude of the recurrent inhibition as observed *in vitro* (see Fig. 4*B*).

A network with a uIPSC decay time of 10 ms and another with a decay of 30 ms were subjected to changes in the uIPSC probability (Fig. 5). Both networks generated fast oscillations in the γ range. However, the frequency of oscillations in the network with slow uIPSCs was lower at all values of uIPSC probability. Therefore, a prolongation of the decay time constant of uIPSCs alone was sufficient to decrease the oscillation frequency of the network. Both networks were also sensitive to a reduction in the amplitude of the uIPSC probability (Fig. 5*A*). Below a certain value of recurrent (and lateral) inhibition, the oscillation frequency followed the average mitral cells firing rate in both networks (Fig. 5*B*). For the network with fast uIPSCs, this process led to a reduction of the oscillation frequency from 60 to 43 Hz (Fig. 5*B*). Thus, a prolongation of uIPSC decay time, as well as a reduction of uIPSC occurrence probability, reduces network oscillation frequency. To assess the validity of these predictions, we recorded γ oscillations of the LFP measured near the mitral cell body layer in acute OB slices.

Gamma Oscillations Are Slower in the OB Network of $\alpha1^{0/0}$ Mice. A brief stimulation of the olfactory nerve terminals (100 μs, 5–60 V) elicited robust fast oscillations in acute OB slices (Fig. 6 *A* and *B*) (for a review, see ref. 27). No significant difference was found in the stability of the LFP oscillations between WT and $\alpha1^{0/0}$ OB slices (Fig. 6*C*). Similarly, mitral cells synchrony tended to be lower in $\alpha1^{0/0}$ mice, as also seen in our model (SI Fig. 11*E*), but no significant difference was found at any stimulation strength (Fig. 6*D*). In contrast, and as predicted by the theoretical model, the frequency of the induced oscillations was much lower in slices from $\alpha1^{0/0}$ mice than in control slices, at all stimulation strengths (Fig. 6*E*) and for several hundreds of milliseconds after the onset of stimulation (Fig. 6*H*). This was not due to an effect on olfactory nerve inputs, as assessed by the measurement of the slope of the field excitatory postsynaptic potential (Fig. 6*F*) measured in the glomerulus or to a reduced activity of mitral cells firing (Fig. 6*G*). Indeed, the olfactory nerve-induced discharge of mitral cells was stronger in $\alpha1^{0/0}$ than in WT mice. Our findings clearly indicate that a reduction

in functional $GABA_A$ receptor-mediated inhibition between local interneurons and mitral cell dendrites, accompanied by slower kinetics, damped down LFP γ oscillations.

Discussion

We show that the removal of the α1-subunit of $GABA_A$ receptors caused a partial loss of functional inhibitory synapses impinging onto mitral cell dendrites, whereas at somatic synapses α1-$GABA_A$ receptors were completely replaced by receptors carrying the α3 subunit. This switch in receptor subunit composition resulted in slower decaying currents of unchanged amplitude. The reduction in the number of functional inhibitory synapses together with altered kinetics led to more variable and slower dendrodendritic inhibition received by mitral cells in $\alpha1^{0/0}$ mice. For the network as a whole, these changes resulted in a much lower oscillation frequency although the strength of olfactory nerve afferent inputs was unchanged. Both experimental and theoretical results demonstrated that a specific targeted alteration of the inhibition received by mitral cells slowed down network oscillations. Therefore, these results highlight the importance of synaptic inhibition mediated by α1-$GABA_A$ receptors located on lateral dendrites of mitral (and tufted) cells, for constraining rhythmic activity in the γ range.

Inhibition Properties and Oscillation Frequency. The α subunit of $GABA_A$ receptors determines the affinity for GABA, the sensitivity for benzodiazepines and the kinetics of activation/deactivation (reviewed in refs. 28 and 29). *In vitro*, $\alpha1^{0/0}$ mice display slower inhibitory synaptic events in distinct neuronal types, such as in cerebellar neurons (23), in hippocampal pyramidal cells and interneurons (30), and in neocortical neurons (31). Consistent with these results, we found that the inhibitory component of dendrodendritic synapses was slower to decay in $\alpha1^{0/0}$ mice. Both experimental and theoretical approaches demonstrated that the slower kinetics of $GABA_A$ receptor-mediated currents caused an increase in the rise time of evoked inhibition received by mitral cells (Fig. 4*E* and SI Fig. 11). This alteration, in turn, reduced the frequency of γ oscillations.

Using intracellular recordings under current-clamp mode, we found differences in the intrinsic properties of mitral cells from WT and $\alpha1^{0/0}$ mice: the latter display higher membrane resistance and a higher excitability (see SI Fig. 12*F*). The increase in the membrane resistance could explain in part the increase in mitral cell excitability. These unexpected modifications may result from a modification of intrinsic conductance (reviewed in ref. 32). Our results obtained from the OB network model indicate that increase in mitral cell excitability tends to enhance the frequency of network oscillations (SI Fig. 13). This modification contrasts sharply with the reduction of oscillation frequency we found and therefore indicates that when comparing oscillations between the two genotypes, our results might underestimate the differences.

Both anatomical and physiological findings suggest the presence of a smaller number of functional inhibitory synapses on mitral cell dendrites. Mimicking this feature in our model by a reduction of GABA release probability resulted in an increase in the variability of recurrent and lateral inhibition onto mitral cells. This modification can destabilize the network to a situation in which the network oscillation frequency follows the mitral cell firing frequency (see SI Fig. 13). We proposed (26) that the frequency of γ oscillations in the OB network is insensitive to modification of the amplitude of $GABA_A$ receptor conductance. Here, we demonstrated that the variability of the lateral inhibition between mitral cells could substantially decrease the oscillation frequency (Fig. 5). Thus, the variability of the lateral inhibition is a more critical determinant for the network oscillations than simply the size of its component unitary GABAergic synaptic events.

Heterogeneity of $GABA_A$ Receptors in Mitral Cells. As seen in rats (22), mitral (and tufted) cells express a complex mixture of α1- and α3-$GABA_A$ receptors, sometimes colocalized in single clusters. Ultrastructurally, both types of $GABA_A$ receptors in reciprocal synapses are present both postsynaptically in symmetric synapses and presynaptically in asymmetric synapses (25). Gephyrin is present only in symmetric synapses, supporting the contention that gephyrin clusters seen by immunofluorescence represent synaptic sites. The present results reveal several unusual features of $GABA_A$ receptors in mitral cells: (*i*) they are highly heterogeneous with respect to subunit composition, notably presence or absence of the γ2 subunit (see SI Table 1); (*ii*) gephyrin clusters are maintained at postsynaptic sites apparently lacking $GABA_A$ receptors in mutant mice; (*iii*) somatic and dendritic synapses differ remarkably in the extent of compensation occurring in the absence of the α1-subunit. The failure of the α3-subunit to form clusters replacing the missing α1-subunit in numerous dendrodendritic reciprocal synapses of $\alpha1^{0/0}$ mice implies that α1 and α3 are not simple interchangeable units at these synapses. This is consistent with results showing that $GABA_A$ receptor α subunit variants coexpressed in the same cell are not functionally exchangeable (33). A possible cause for the subunit heterogeneity of $GABA_A$ receptors is the continuous "recycling" of GABAergic synapses in the EPL due to the replacement of granule cells by newly differentiated cells. Therefore, we propose that synapses lacking the γ2-subunit are either immature or senescent.

Are all Synapses Between Mitral and Granule Cells Really Reciprocal? The heterogeneity of inhibitory synapses on mitral cells might also come from the diversity of their function within the same presynaptic partners. Proximal reciprocal synapses have the ability to control mitral cell firing, whereas distal reciprocal synapses control action potential propagation (34) and collect information from neighboring mitral cells. In terms of lateral inhibition, neither proximal nor distal synaptic contacts are bidirectional. Distal dendrodendritic synapses collect the excitation coming from a large subset of mitral cells, whereas proximal reciprocal synapses control activity of mitral cell clusters receiving the same sensory inputs. The recent finding of a columnar organization of granule cells around mitral cells putatively connected to the same glomerulus support this idea (35). According to this view, granule cells in an individual functional column might collect information from mitral cell dendrites crossing that region, and in turn, preferentially inhibit the mitral cells whose cell bodies are located within the column.* Even if purely speculative, this view could be relevant for the analysis of the phenotype of $\alpha1^{0/0}$ mice. In both WT and $\alpha1^{0/0}$ mice, we found the same density of gephyrin clusters. Additionally, we found that gephyrin was always localized to postsynaptic specializations of symmetric synapses. These results suggest that the excitatory component from mitral to granule cells could still be functional in $\alpha1^{0/0}$ mice. Thus, granule cells in $\alpha1^{0/0}$ mice could still collect information from virtually the same amount of mitral cells. In turn, the integration of these inputs could serve to inhibit mitral cells around their soma at which location inhibitory synapses are still functional. The dramatic loss of inhibitory synapses on mitral cell dendrites of $\alpha1^{0/0}$ mice might not have drastic consequences on granule cell information collection and consequent mitral cell body inhibition within an OB column, but may rather impact on the fine regulation of information distribution between columns.

Making Sense of γ Oscillations in the Olfactory System. Oscillations in the γ range correlate with discrimination in rodents (3). In the olfactory cortex, the summation between inputs occurs within intervals shorter than 10 ms, which corresponds to the duration of half a cycle of γ oscillation (36). This property could be determined by the intrinsic properties of pyramidal cells (36) and/or by a feed-forward inhibition (37). The fast rhythmic synchronization present in both the bulbar and cortical circuits, along with intrinsic

*Migliore, M., Shepherd, G.M. (2006) *Soc. Neurosci. Abstr.* 797:15 (abstr.).

neuronal properties, may thus define precise integration frames for cortical pyramidal cells. Consequently, in combination with the convergence of mitral cell projections, γ oscillations allow the integration of the sensory information that is spread throughout the mitral cell population. Alternative mechanisms have been proposed to account for stimuli discrimination in the olfactory system. A phase coding of mitral cell spikes on θ oscillations (1–10 Hz) has been suggested to encode both odor intensity and identity (38–42). The relative latency of discharge among mitral cells apparently provides a suitable device for odor identification and could explain the short duration required for odor discrimination in rodents (43–45). Finally, it is worth mentioning that a slow decorrelation of mitral cell discharge patterns has been proposed as well to support odor identification (46).

Discrimination and identification processes of odorant information (47) do not depend on mitral cells inhibition to the same extent, so future experimental and theoretical approaches that will take into account the diversity of functions of GABAergic synapses provided by the local inhibitory interneurons might give us insight into olfactory sensory information encoding.

Materials and Methods

Homozygous $\alpha1^{0/0}$ mice were generated in a mixed C57BL/6J-129Sv/SvJ background (23). All analyses were performed in homozygous animals obtained by intercrossing heterozygous mutants or homozygotes from F_1 breeding pairs. The experiments were approved by the local authorities and were performed in accordance with the European Community Council Directive (86/609/EEC) and the institutional guidelines of the Pasteur Institute and of the Universities of Turin and Zurich.

Immunofluorescence Staining. Double and triple immunofluorescence staining was performed on sections prepared from frozen tissue as described in ref. 22. Primary antibodies against the $GABA_A$ receptor $\alpha1$-subunit (rabbit or guinea pig), $\alpha2$-, $\alpha3$-, $\alpha5$-, $\gamma2$-subunits (guinea pig; see ref. 21), and gephyrin (monoclonal mAb7a; Synaptic Systems, Göttingen, Germany) were used in various combinations.

Immunoelectron Microscopy. OB tissues were obtained from mice used in a previous study (48). Postembedding immunogold labeling for GABA was performed on ultrathin sections of tissue embedded in Epon, and labeling for gephyrin and the $\alpha3$-subunit was performed in sections of Lowicryl-embedded tissue. All procedures were performed as described in ref. 48. Rabbit polyclonal antibodies against GABA (1:200) (Sigma, St Louis, MO) and against gephyrin (1:4,000; recognizing all gephyrin isoforms; see ref. 49 for characterization), and guinea pig anti-$\alpha3$-subunit antibody (6 μg/ml; affinity purified) were used.

Electrophysiology. OB slices from adult mice (1–4 months old) were prepared as described in ref. 9. Patch-clamp recordings were performed with glass micropipettes filled with 132 mM CsCl, 8 mM NaCl, 0.2 mM CsEGTA, 10 mM Na-Hepes, 10 mM glucose, and 1 mM $MgCl_2$ (pH 7.4, 280 mosmol), which had resistances of 4–7 MΩ. Slices were perfused at room temperature with normal aCSF, containing 5 mM kynurenate and 10 μM gabazine to block ionotropic glutamate receptors and $GABA_A$ receptors, respectively. Dendrodendritic responses were elicited by brief depolarizing steps (from -70 mV to $+20$ mV, 50 ms) in Mg-free solution containing 1 μM tetrodotoxin. Intracellular and extracellular recordings were performed as described in ref. 9.

Model. The OB network was modeled by an array of 10×10 mitral cells as described in ref. 26. The $\alpha1^{0/0}$ phenotype was modeled by reducing both the decay time constant of uIPSCs and the release probability peak amplitude according to the anatomical and physiological data presented in the results section. None of the other parameters were modified.

We thank G. Homanics (University of Pittsburgh) for providing $\alpha1^{0/0}$ mice, G. Schwarz (University of Cologne) for the antibody against gephyrin, J. Kralic for his contribution during the initial phases of the project and help with breeding, and C. Sidler and F. Parpan for excellent technical assistance. This work was supported by the Fondation pour la Recherche Médicale, the Fédération pour la Recherche sur le Cerveau, Agence Nationale de la Recherche Grant ANR-05-Neur-028-01 (to P.-M.L), a fellowship from the Centre National de la Recherche Scientifique (to R.E.R.), Swiss National Science Foundation Grant 3100A0-108260 (to J-M.F.), Regione Piemonte bando 2004-A218, and Ministero dell'Istruzione, dell'Università e della Ricerca Italia Grant PRIN 2005059123 002 (to M.S.P.).

1. Laurent G, Stopfer M, Friedrich RW, Rabinovich MI, Volkovskii A, Abarbanel HD (2001) *Annu Rev Neurosci* 24:263–297.
2. Urban N, Egger V (2006) *Semin Cell Dev Biol* 17:424–432.
3. Nusser Z, Kay LM, Laurent G, Homanics GE, Mody I (2001) *J Neurophysiol* 86:2823–2833.
4. Ravel N, Chabaud P, Martin C, Gaveau V, Hugues E, Tallon-Baudry C, Bertrand O, Gervais R (2003) *Eur J Neurosci* 17:350–358.
5. Martin C, Gervais R, Messaoudi B, Ravel N (2006) *Eur J Neurosci* 23:1801–1810.
6. Gray CM, Skinner JE (1988) *Exp Brain Res* 69:378–386.
7. Neville KR, Haberly LB (2003) *J Neurophysiol* 90:3921–3930.
8. Friedman D, Strowbridge BW (2003) *J Neurophysiol* 89:2601–2610.
9. Lagier S, Carleton A, Lledo PM (2004) *J Neurosci* 24:4382–4392.
10. Chen WR, Shepherd GM (1997) *Brain Res* 745:189–196.
11. Desmaisons D, Vincent JD, Lledo PM (1999) *J Neurosci* 19:10727–10737.
12. Carlson GC, Shipley MT, Keller A (2000) *J Neurosci* 20:2011–2021.
13. Schoppa NE, Westbrook GL (2002) *Nat Neurosci* 5:1194–1202.
14. Christie JM, Bark C, Hormuzdi SG, Helbig I, Monyer H, Westbrook GL (2005) *Neuron* 46:761–772.
15. Rall W, Shepherd GM, Reese TS, Brightman MW (1966) *Exp Neurol* 14:44–56.
16. Rall W, Shepherd GM (1968) *J Neurophysiol* 31:884–915.
17. Mori K, Takagi SF (1978) *J Physiol* 279:569–588.
18. Price JL, Powell TPS (1970) *J Cell Sci* 7:157–187.
19. Davis BJ, Macrides F (1981) *J Comp Neurol* 203:475–493.
20. Barnard EA, Skolnick P, Olsen RW, Mohler H, Sieghart W, Biggio G, Braestrup C, Bateson AN, Langer SZ (1998) *Pharmacol Rev* 50:291–313.
21. Fritschy JM, Mohler H (1995) *J Comp Neurol* 359:154–194.
22. Panzanelli P, Perazzini AZ, Fritschy JM, Sassoè-Pognetto M (2005) *J Comp Neurol* 484:121–131.
23. Vicini S, Ferguson C, Prybylowski K, Kralic J, Morrow AL, Homanics GE (2001) *J Neurosci* 21:3009–3016.
24. Giustetto M, Kirsch J, Fritschy JM, Cantino D, Sassoè-Pognetto M (1998) *J Comp Neurol* 395:231–244.
25. Panzanelli P, Homanics GE, Ottersen OP, Fritschy JM, Sassoè-Pognetto M (2004) *Eur J Neurosci* 20:2945–2952.
26. Bathellier B, Lagier S, Faure P, Lledo PM (2006) *J Neurophysiol* 95:2678–2691.
27. Lledo PM, Lagier S (2006) *Semin Cell Dev Biol* 17:443–453.
28. Sieghart W, Sperk G (2002)*Curr Top Med Chem* 2:795–816.
29. Korpi ER, Grunder G, Luddens H (2002) *Prog Neurobiol* 67:113–159.
30. Goldstein PA, Elsen FP, Ying SW, Ferguson C, Homanics GE, Harrison NL (2002) *J Neurophysiol* 88:3208–3217.
31. Bosman LW, Heinen K, Spijker S, Brussaard AB (2005) *J Neurophysiol* 94:338–346.
32. Turrigiano GG, Nelson SB (2004) *Nat Rev Neurosci* 5:97–107.
33. Kralic JE, Sidler C, Parpan F, Homanics G, Morrow AL, Fritschy JM (2006) *J Comp Neurol* 495:408–421.
34. Xiong W, Chen WR (2002) *Neuron* 34:115–126.
35. Willhite DC, Nguyen KT, Masurkar AV, Greer CA, Shepherd GM, Chen WR (2006) *Proc Natl Acad Sci USA* 103:12592–12597.
36. Franks KM, Isaacson JS (2006) *Neuron* 49:357–363.
37. Neville KR, Haberly LB (2004) in *The Synaptic Organization of the Brain*, ed Shepherd GM (Oxford Univ Press, New York), 3rd Ed, pp 415–454.
38. Li Z, Hopfield JJ (1989) *Biol Cybern* 61:379–392.
39. Hopfield JJ (1995) *Nature* 376:33–36.
40. Cang J, Isaacson JS (2003) *J Neurosci* 23:4108–4116.
41. Margrie TW, Schaefer AT (2003) *J Physiol* 546:363–374.
42. Schaefer AT, Angelo K, Spors H, Margrie TW (2006) *PLoS Biol* 4:e163.
43. Uchida N, Mainen ZF (2003) *Nat Neurosci* 6:1224–1229.
44. Abraham NM, Spors H, Carleton A, Margrie TW, Kuner T, Schaefer AT (2004) *Neuron* 44:865–876.
45. Rinberg D, Koulakov A, Gelperin A (2006) *Neuron* 51:351–358.
46. Friedrich RW, Habermann CJ, Laurent G (2004) *Nat Neurosci* 7:862–871.
47. Rinberg D, Gelperin A (2006) *Semin Cell Dev Biol* 17:454–461.
48. Fritschy JM, Panzanelli P, Kralic JE, Vogt KE, Sassoè-Pognetto M (2006) *J Neurosci* 26:3245–3255.
49. Giesemann T, Schwarz G, Nawrotzki R, Berhörster K, Rothkegel M, Schlüter K, Schrader N, Schindelin H, Mendel RR, Kirsch J, *et al.* (2003) *J Neurosci* 23:8330–8339.